Star Formation and Tidal Encounters with the Low Surface Brightness Galaxy UGC 12695 and Companions

K. O'Neil[1], M.A.W. Verheijen[2], S.S. McGaugh[3]

[1]Arecibo Observatory, HC03 Box 53995, Arecibo, PR 00612, email:koneil@naic.edu
[2]National Radio Astronomy Observatory, Box 0, Socorro, NM 87801, email:mverheij@nrao.edu
[3]Department of Astronomy, University of Maryland, College Park, MD 20742, email:ssm@astro.umd.edu

ABSTRACT– We present VLA H I observations of the low surface brightness galaxy UGC 12695 and its two companions, UGC 12687 and a newly discovered dwarf galaxy 2333+1234. UGC 12695 shows solid body rotation but has a very lopsided morphology of the H I disk, with the majority of the H I lying in the southern arm of the galaxy. The H I column density distribution of this very blue, LSB galaxy coincides in detail with its light distribution. Comparing the H I column density of UGC 12695 with the empirical (but not well understood) value of $\Sigma_c = 10^{21}$ atoms cm^{-2} found in, i.e., Skillman's 1986 paper shows the star formation to be a local affair, occurring only in those regions where the column density is above this star formation threshold. The low surface brightness nature of this galaxy could thus be attributed to an insufficient gas surface density, inhibiting star formation on a more global scale. Significantly, though, the Toomre criterion places a much lower critical density on the galaxy ($\sim 10^{20}$ atoms cm^{-2}), which is shown by the galaxy's low SFR to not be applicable.
Within a projected distance of 300 kpc/30 km sec^{-1} of UGC 12695 lie two companion galaxies – UGC 12687, a high surface brightness barred spiral galaxy, and 2333+1234, a dwarf galaxy discovered during this investigation. The close proximity of the three galaxies, combined with UGC 12695's extremely blue color and regions of localized starburst and UGC 12687's UV excess bring to mind mutually induced star formation through tidal activity.

Subject headings: galaxies: individual(UGC 12695, UGC 12687, 2333+1234) – galaxies: spiral – galaxies: evolution – galaxies: interactions – galaxies: kinematics and dynamics – galaxies: structure

1 Introduction

Attempts to understand star formation in low surface brightness (LSB) galaxies has resulted in a large number of theories being discarded and few alternatives being offered. As a result we have considerable knowledge on what these enigmatic systems are not. LSB galaxies are *not*:

- simply the faded version of high surface brightness (HSB) galaxies. Although some red LSB galaxies have been found which may be the end product of the faint blue galaxies, the majority of LSB galaxies have very blue colors and low metallicities (i.e. Ferguson & McGaugh 1995; O'Neil, *et.al.*1997a; McGaugh 1994; Schombert, *et.al.*1990; De Blok & Van der Hulst 1998), arguing against any fading scenario.
- lacking the neutral hydrogen necessary to form stars, as many LSB galaxies contain more than 10^9 $M_\odot$ of H I and LSB galaxies include some of the highest M_{HI}/L_B galaxies known (O'Neil, Bothun, & Schombert 1999).
- a completely new type of galaxy. The transition from HSB to LSB galaxies is smooth, with LSB galaxies covering the entire color and morphological spectrum of HSB galaxies (i.e. O'Neil, *et.al.*1997b; Matthews & Gallagher 1997)

[0]To be published in The Astronomical Journal, May 2000

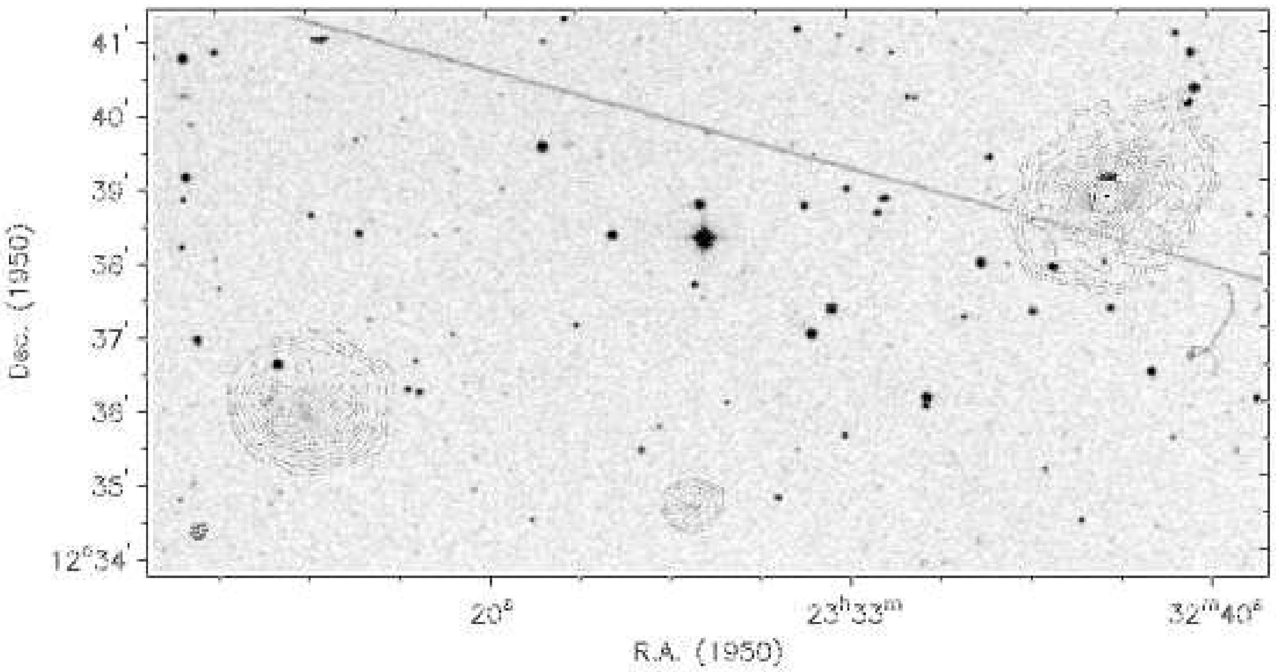

Figure 1: H I contours of all three galaxies overlaid on a POSS-II image.

UGC 12695 is a relatively nearby (z=0.021) low surface brightness galaxy with an absolute blue magnitude of M_B=−18.9. Previous studies of UGC 12695 (McGaugh, 1994; O'Neil *et.al.*, 1998) have shown it to be very remarkable. The galaxy is of an exceedingly transparent nature, evidenced by the many background galaxies seen through its elusive disk, and it contains a reasonably high gas fraction (M_{HI}/L_B = 2.6 $M_\odot$ /$L_\odot$) while having a very low metallicity and an extremely blue color for a galaxy ($U-I=-0.2$) (Table 1).

Because UGC 12695 was thought to be fairly isolated, with the nearest galaxy (UGC 12687) lying more than 277 kpc away (Figure 1), it provides a good opportunity for studying star formation and evolution in LSB galaxies. To this end, and with the above points in mind, we undertook to observe UGC 12695 with the Very Large Array (VLA) in the C configuration. The results of these observations are described in this paper, as follows: Section 2 describes the observations and data reduction; Section 3 examines the H I morphology and kinematics of UGC 12695 and its companions – UGC 12687, and 2333+1234; Section 4 looks at the dark and visible mass of UGC 12695; Section 5 examines the star formation potential of UGC 12695; Finally, section 6 examines the possibility of a recent tidal encounter between the UGC galaxies.

Table 1: Global properties of UGC 12695 and UGC 12687.

		UGC 12695	UGC 12687
Type		Sm[1]	SBbc[1]
V_{hel}	km s^{-1}	6186[2]	6150[2]
M_B	mag	-18.9[3]	-20.3[1]
$B-V$		0.26[3]	0.70[4]
$\mu_B(0)$	mag/arcsec^2	23.8[3]	-
r_{25}	kpc	0.79[1]	0.87[1]
M_{HI}	$M_\odot$	7.5×10^9 [2]	1.2×10^{10} [2]
M_{HI}/L_B	$M_\odot/L_\odot$	2.62[2]	1.18[2]

[1]De Vaucouleurs, *et.al.*1991
[2]This paper
[3]O'Neil, *et.al.*1998
[4]Prugniel & Heraudeau 1998

2 The Data – Observations and Reduction

H I spectral line synthesis observations of UGC 12695 and its companions were done in two runs with the VLA in its new C-short configuration and are specified in Table 2. The primary calibrator 3C48 was observed three times per run and the secondary phase calibrator

Table 2: VLA observing parameters

Configuration		C-short
Correlator mode		2AC-normal
Total integration time	(hours)	15.5
Dates of observation		15Jan99
		16Jan99
Field center, α(B1950)		23:33:30
δ(B1950)		12:35:53
Central frequency	(MHz)	1391.64
$V_{\rm hel}$ of central channel	(km s^{-1})	6170
Primary beam FWHM	(arcmin)	32.4
Synthesized beam ($\alpha\times\delta$)	(arcsec)	16.2$\times$14.1
Bandwidth	(MHz)	1.5625
Number of channels		256
Channel separation	(km s^{-1})	1.31
Velocity resolution	(km s^{-1})	1.58
rms noise in one channel	(K)	2.63
K-mJy conversion, equiv. of 1mJy/beam	(K)	2.76

2340+135 was observed every 35 minutes.

Calibration, flagging, concatenation and Fourier transformation of the UV data was done with the AIPS package. A robust R=0 weighting of the UV data points was applied and the entire primary beam was imaged with a 512 x 512 map of 5 arcsecond pixels. The dirty maps and corresponding antenna patterns were exported into the GIPSY package which was used for further data reduction and analysis as described below.

The number of velocity channels was reduced by averaging adjacent pairs of channel maps which resulted in a data cube of 127 nearly independent channels, each 2.68 km sec^{-1} wide. The dirty maps were cleaned down to half the rms noise level with channel dependent search areas using the standard Högbom algorithm. The clean components were restored with a Gaussian beam of FWHM 16.2$\times$14.1 arcsec at a position angle of −54 degrees. The data cube was then Hanning smoothed in velocity which resulted in a velocity resolution of 5.3 km sec^{-1} .

No continuum emission was detected in the averaged line-free channels at the positions of UGC 12695 and 2333+1234. Due to a steep rotation curve, the line emission at the center of UGC 12687 spans the entire bandpass, leaving only 4 line-free continuum channels at the high velocity end of the data cube while some line emission at the low velocity edge of the bandpass is severely affected by the high noise level. No continuum emission could be detected in the line-free channels at the position of the disk of UGC 12687. Therefore, no continuum map was subtracted to avoid the unnecessary addition of noise to the channel maps and the nuclear continuum emission of UGC 12687 was removed at a later stage.

The areas of H I emission were isolated in each channel map and the pixels outside these areas were set to zero. Global H I profiles were derived by measuring the total flux in the isolated areas, corrected for primary beam attenuation. In the case of UGC 12687, a 2.9 mJy baseline was subtracted from the global profile.

Integrated H I maps of the galaxies were constructed by summing the primary beam corrected, isolated areas of H I emission. At the position of the nucleus of UGC 12687, 7 channels at the high velocity end of the data cube are free from line emission and those were averaged to obtain a map of the central continuum source. A Gaussian beam was fitted to this source, giving a primary beam corrected flux density of 2.9$\pm$0.2 mJy at the position $23^{\rm h}32^{\rm m}45^{\rm s}.4$ and $23^{\rm d}32'53''$ (B1950). Subsequently, this fitted Gaussian was subtracted from the integrated H I map.

Velocity fields were constructed by fitting a single Gaussian to each profile and rotation curves for UGC 12695 and UGC 12687 were derived by fitting tilted rings of 11 arcsec width to their velocity fields.

Optical images were taken from the Hubble Space Telescope Wide Field Planetary Camera-2 (WFPC2) images of O'Neil, *et.al.*(1998), the MDM 1.3m McGraw Hill telescope (McGaugh, Schombert, & Bothun 1995), and from the Space Telescope Science Institute Digital Sky Survey. The metallicity studies of UGC 12695 are from McGaugh (1994).

H_0 is 75 km s^{-1} Mpc^{-1} throughout this paper, and a Virgo-centric infall of 300 km s^{-1} is assumed. B1950 coordinates are used throughout this paper.

3 H I morphology and kinematics

The following subsections contain detailed descriptions of the overall properties of the neutral hydrogen gas in UGC 12695 and its companions UGC 12687 and 2333+1234 which are illustrated in Figures 2, 3, 4, respectively. The beam size is 16.2” $\times$ 14.1”, or 6.4 kpc $\times$ 5.6 kpc at 82 Mpc.

3.1 UGC 12695

Figure 2 presents the data of UGC 12695. The upper left panel displays the HST WFPC2 F814W image of O'Neil, *et.al.* (1998). It shows a relatively smooth triangular inner region and an irregular outer disk dominated by several large star forming Hα regions. Several background galaxies can be seen through the disk, evidencing its extremely transparent nature. The southern spiral arm seems to be sharply outlined while the northern arm is extremely diffuse. Smoothing the WFPC2 image to a $1''$ resolution and fitting an ellipse to the faintest isophotes indicates a position angle of 88°, an

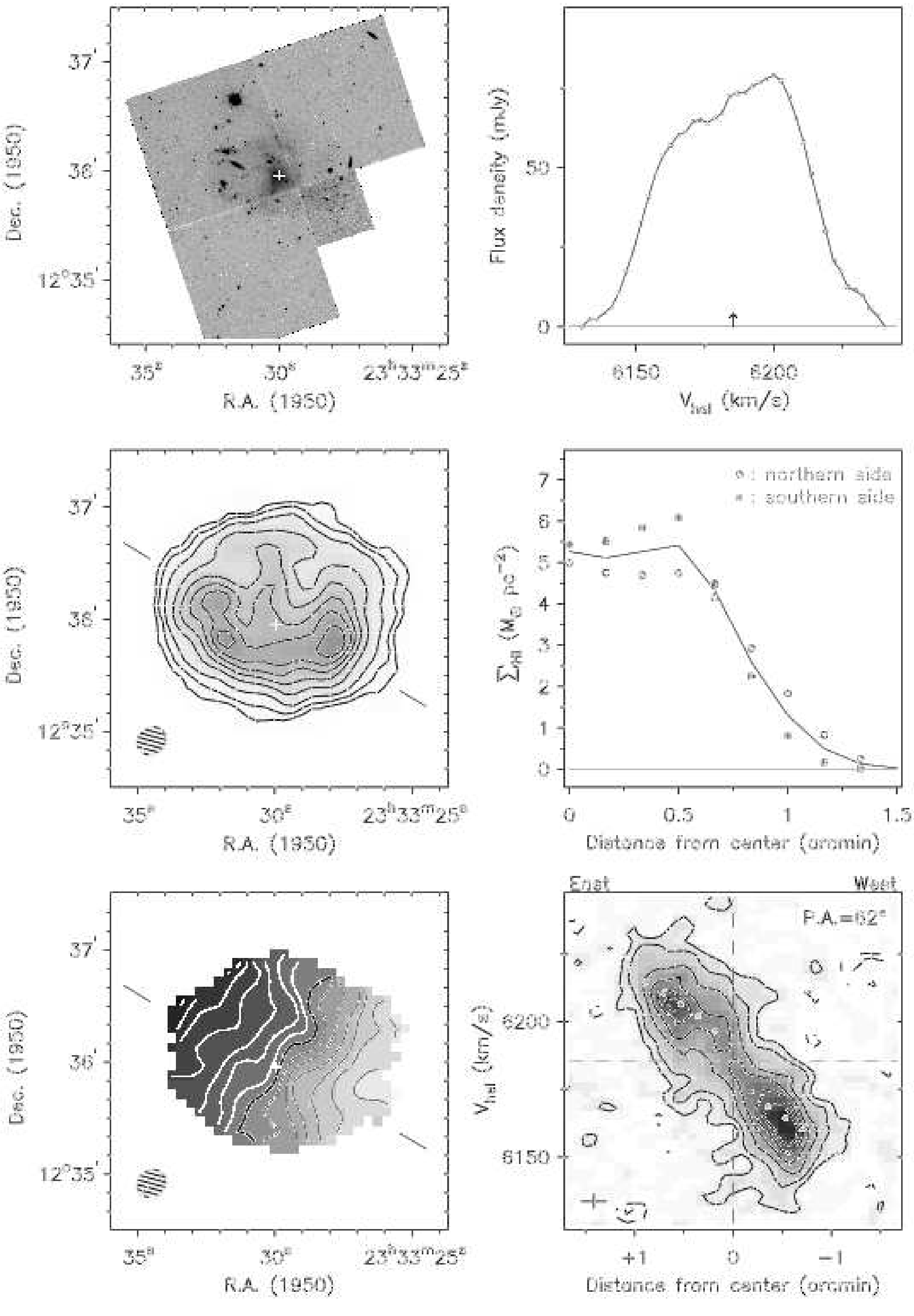

Figure 2: UGC 12695. See section 3.1 for explanations.

inclination of 43° and a central position at ($23^h33^m30.4^s$, 12°36′1″).

The upper right panel shows the global H I profile obtained by measuring the flux in the individual channel maps. The width at the 20% level of the peak flux is 79.4 km sec^{-1} and the width at the 50% level of the peak flux is 62.2 km sec^{-1}. The integrated flux density is 4.7 Jy km s^{-1} which corresponds to a total H I mass of 7.5×10^9 $M_\odot$ for a distance of 82 Mpc (v=6186 km s^{-1} (Table 1) and H_0=75 km s^{-1} Mpc^{-1}). The shape of the profile suggests a global lopsidedness of the H I distribution and or kinematics. The vertical arrow indicates the systemic velocity as derived from the H I velocity field. It should be noted that the H I profile of UGC 12695 was previously determined both by Theureau, *et.al.* (1998) using the Nançay telescope and Schneider, *et.al.*(1990) using the Arecibo telescope. Although both of the earlier observations match our velocity widths, the Nançay result list a 40% smaller total flux. As our results match those of Schneider, *et.al.*, we believe the data differences to be the result of uncertain beam shapes and primary beam corrections in the Nançay data.

The middle left panel presents the integrated H I column density map with the size of the synthesized beam in the lower left corner. This H I map is at the same scale as the WFPC2 image above. Contour levels are drawn at 0.5, 1, 2, 4, 6, 8, 10 and 12×10^{20} atoms cm^{-2}. Overall, the neutral hydrogen distribution of UGC 12695 appears to match the optical morphology quite well, including the fact that the H I distribution is very lopsided with a high column density ridge running through the southern part of the disk. The cross corresponds to the position of the cross in the WFPC2 image and indicates the central optical concentration. Fitting an ellipse to the lowest H I contours indicates a position angle of 80°, an inclination of 37° after a first order beam smearing correction, and puts the center of the H I disk at ($23^h33^m30.0^s$, 12°36′4″), 7 arcseconds ($<$ 1 beam width) north of the central optical concentration.

The middle right panel shows the radial H I column density distribution, azimuthally averaged over the northern and southern sides separately. Clearly, the H I surface density falls off more sharply at the southern edge, going from 10 to 0.5 x 10^{20} atoms cm^{-2} within two beam widths.

The lower left panel shows the H I velocity field. Apart from some obvious wrinkles due to non-circular or streaming motions, the velocity field is dominated by solid body rotation. This makes it impossible to determine the dynamical center and inclination from the velocity field and therefore the optical center (cross) was adopted as the dynamical center. The thick line indicates the adopted systemic isovelocity contour at 6185.7 km sec^{-1} while the black contours indicate the approaching side and the white contours the receding side of the galaxy. The isovelocity contour intervals are set at $\pm n\times5$ km sec^{-1}.

The lower right panel presents the position-velocity diagram along the kinematic major axis. Contours are drawn at -4, -2 (dashed), 2, 4, 8, 12, 16 and 20 times the rms noise level. The vertical dashed line corresponds to the position of the cross in the left panels, the horizontal dashed line corresponds to the adopted systemic velocity. The cross in the lower left corner indicates the beam. All profiles in the vertical direction can be well described by single Gaussians. No double profiles are observed. The solid points show the derived rotation curve projected onto the position-velocity diagram. The rotation curve was derived by fitting full tilted rings to the velocity field, effectively azimuthally averaging the wrinkles. Consequently, this azimuthally averaged rotation curve might deviate locally from the position-velocity slice.

The rotation curve of UGC 12695 is tabulated in Table 3. Fitting a single, galaxy wide ring to the entire velocity field gives a position angle of the kinematic major axis of 62 degree. The short thin lines outside the velocity field indicate this average kinematic major axis. Note the significant difference of 18 degrees between the kinematic and morphological position angles of the outer H I disk. An inclination of 40° is adopted which is the average of the optical and H I inclinations. Given this rather face-on orientation of the disk, the uncertainty in the position of the dynamical center and the obvious deviations from circular motions, we estimate the uncertainties in the rotation curve at some 20%.

3.2 UGC 12687

The upper left panel of Figure 3 shows the blue POSS-II image of UGC 12687, a strongly barred two-armed spiral. The bar dynamics efficiently feeds gas to the nuclear region where a radio continuum source with a peak flux of 4.0±0.6 mJy is found at 1.4 GHz (Condon *et al*, 1998). An ultra-violet excess has been reported by Kazarian & Kazarian (1985), suggesting a high level of star formation activity. Nevertheless, the B–V=0.70 color from Prugniel & Heraudeau (1998) of UGC 12687 is considerably redder than that of UGC 12695.

The upper right panel shows the global H I profile which displays the classical double-horned shape. Fluxes were measured in individual channel maps including the central continuum source. Afterwards, a 2.9 mJy/beam continuum baseline was subtracted from the global profile. Unfortunately, H I emission at the lower velocities is lost in the edge of the passband. To estimate total fluxes and line widths, the high velocity edge was mirrored and, as an educated guess, put in place of the missing low velocity side of the profile.

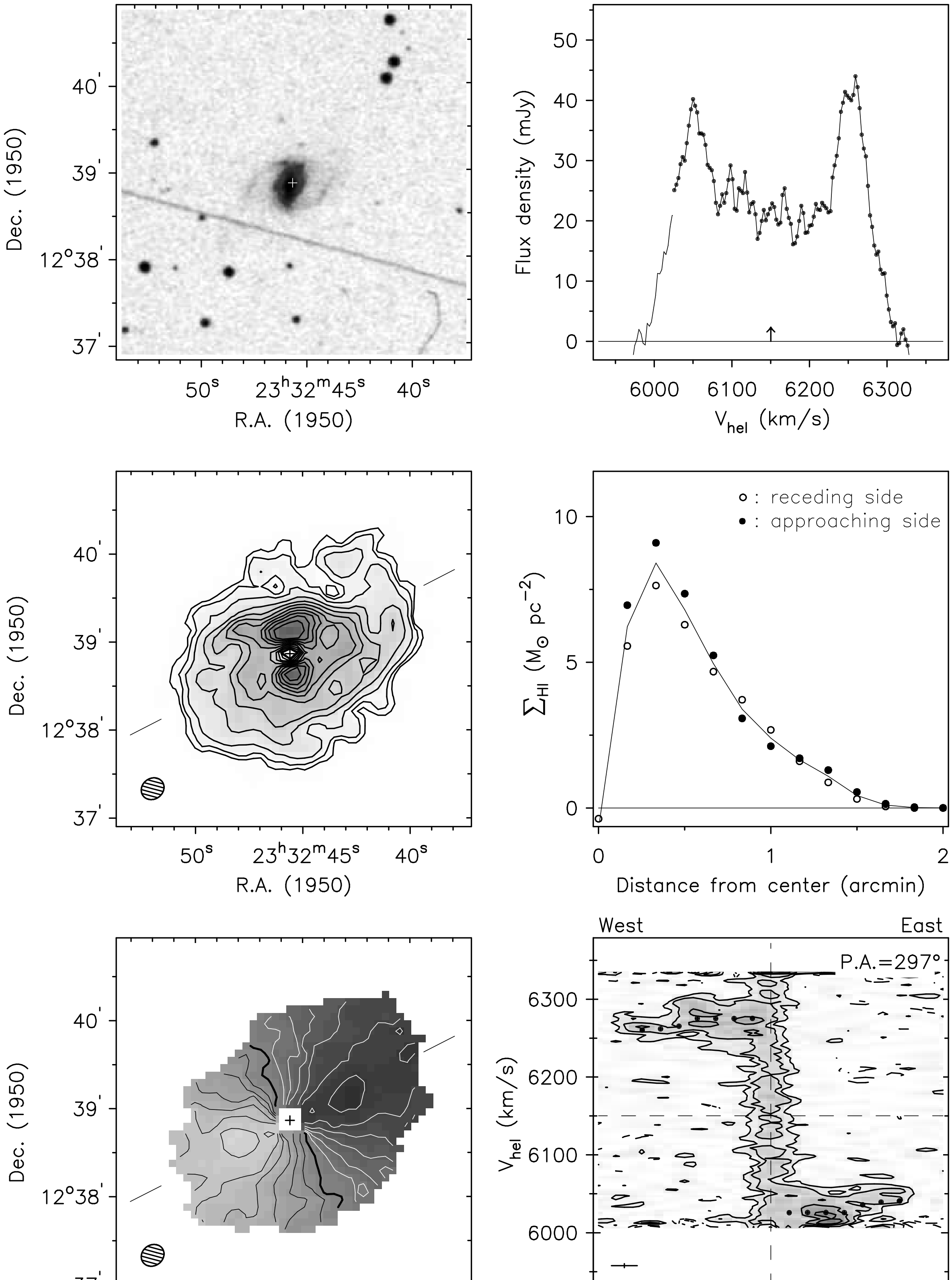

Figure 3: UGC 12687. See section 3.2 for explanations.

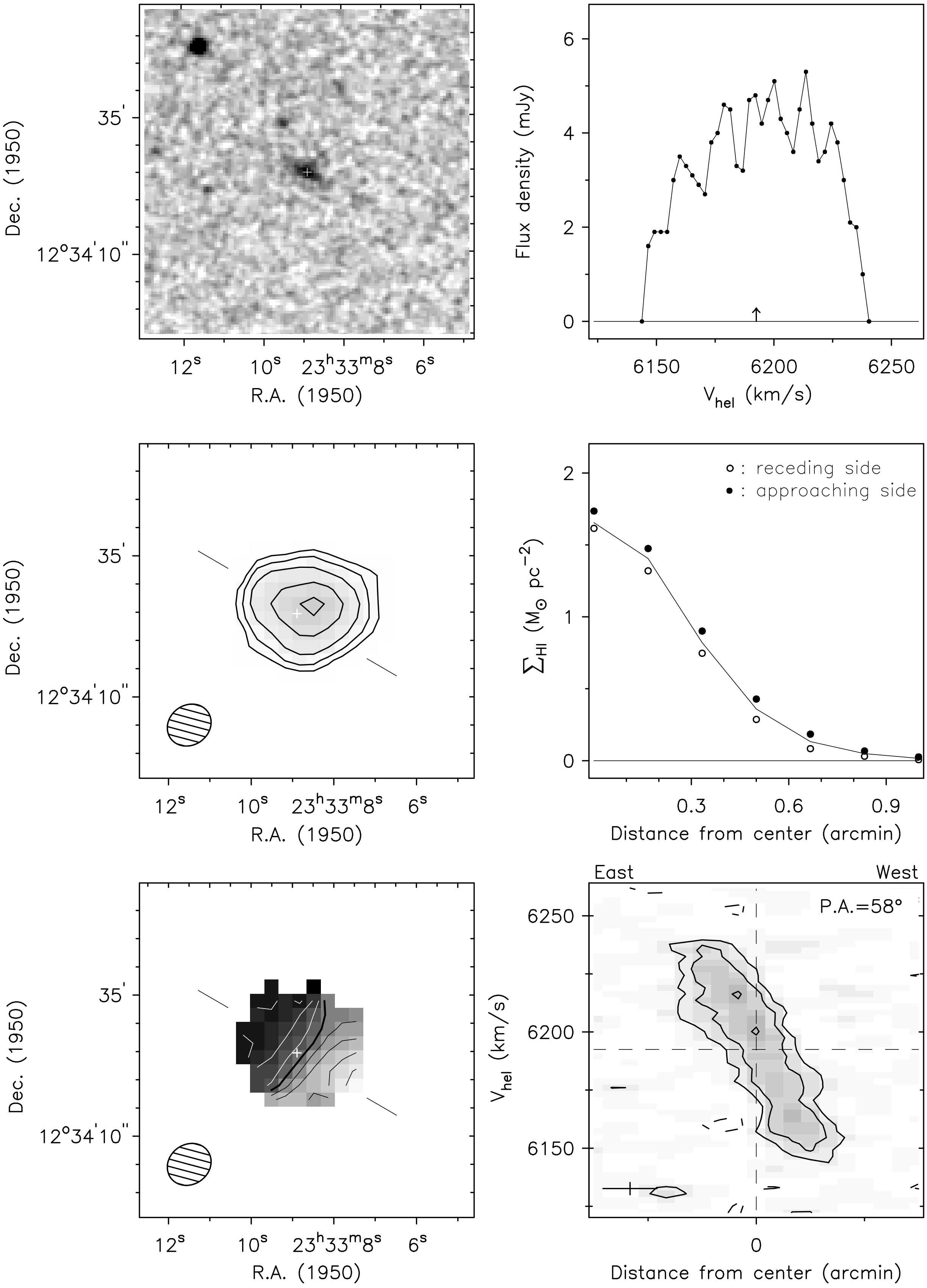

Figure 4: 2333+1234. See section 3.3 for explanations.

This technique gives an integrated flux density of 7.5 Jy km s^{-1} or a total H I mass of 1.2×10^{10} $M_\odot$. The inferred line widths are 296.7 km sec^{-1} at the 20% level and 255.4 km sec^{-1} at the 50% level. Like UGC 12695, UGC 12687 was imaged by Theureau, *et.al.* (1998) with the Nançay telescope, with similar results – the velocity widths of the Nançay data matched ours well, but the total flux reported by Theureau, *et.al.* was only 80% of our result. To check our data, we obtained a 5 minute ON/OFF pair with the Arecibo telescope using the L-narrow receiver. The Arecibo data and our VLA data again matched to within 5% in total flux.

The middle left panel displays the integrated column density map of UGC 12687 constructed by adding the individual channel maps, including the central continuum source which was removed by subtracting a 2.9 mJy/beam central point source. Contour levels are drawn at 0.5, 1, 2, 4, 6, 8, 10, 12, 14, 16 and 18×10^{20} atoms cm^{-2}. The central hole in the H I map might be due to a slight overestimation of the continuum flux or might be caused by H I seen in absorption. Furthermore, the approaching south-eastern side of the galaxy is missing some flux in the integrated H I map due to the bandpass effect mentioned above. Nevertheless, it is clear that the H I gas in UGC 12687 is concentrated near the tips of the bar and to some extent along both optically visible spiral arms. Fitting an ellipse to the outer H I contours gives an axis ratio of (b/a)=0.72 and a position angle of 129.8 degrees centered on ($23^h32^m45.2^s$, $12°38'54''$).

The middle right panel shows the azimuthally averaged radial H I surface density profiles of the receding and approaching sides separately. Note that the approaching side misses some flux around a radius of 1 arcminute.

The lower left panel shows the velocity field which suggests, at least in projection, a declining rotation curve in the inner regions. Fitting tilted rings gives a dynamical center at ($23^h32^m45.4^s$, $12°38'52''$), a systemic velocity of 6150.2 km sec^{-1} (thick line), an inclination of 43° and a position angle of 297°. However, due to the strong bar, non-circular motions are certainly present. No significant warp could be detected. The isovelocity contours are plotted at intervals of $\pm n\times20$ km sec^{-1}. The inferred rotation curve of UGC 12687 is tabulated in Table 3.

The lower right panel shows the position-velocity diagram over the entire observed bandwidth along the kinematic major axis. The central continuum source has not been removed. Note how the low velocity gas is lost in the edge of the bandpass as well as the limited number of line free channels at the high velocity side. Also note the occasional double profiles.

Table 3: Inclination corrected rotation curves of UGC 12695 and UGC 12687.

	UGC 12695			UGC 12687		
R	V_{rot}	incl.	P.A.	V_{rot}	incl.	P.A.
$''$	km/s	$\circ$	$\circ$	km/s	$\circ$	$\circ$
10.7	17	40	62	195	43	297
21.3	26	40	62	195	43	297
32.0	32	40	62	195	43	297
42.7	38	40	62	195	43	297
53.3	45	40	62	179	43	297
64.0	52	40	62	174	43	297
74.7				171	43	297

3.3 2333+1234

In the VLA data cube, the H I emission of a tiny irregular dwarf low surface brightness galaxy was discovered. Having discovered it first in H I, we were then able to discern the galaxy as a barely visible smudge on the POSS-II plate (left panel of Figure 4). Fitting an ellipse to the faintest POSS-II isophotes yields a size of 17.5×7.2 arcsec and a position angle of 58°, centered on ($23^h33^m8.9^s$, $12°34'39''$).

The upper right panel shows the measured global H I profile with an integrated flux of 0.33 Jy km s^{-1} or a total H I mass of 5.2×10^8 $M_\odot$. The line widths are 92 km sec^{-1} at the 20% level and 75 km sec^{-1} at the 50% level.

The middle left panel shows the resolved integrated H I column density map which seems to be slightly offset from the optical image. H I contours are plotted at 0.5, 1, 2, 4 and 6×10^{20} atoms cm^{-2}

The middle right panel shows the barely resolved radial H I surface density profile. No deconvolution attempt was made.

The lower left panel shows the velocity field which clearly indicates a velocity gradient along the optical major axis. The optical center was taken to be the dynamical center and a systemic velocity of 6192.5 km sec^{-1} was inferred. Isovelocity contours are plotted in steps of $\pm n\times10$ km sec^{-1}. Obviously, trying to derive a rotation curve by fitting tilted rings is futile.

The lower right panel displays the position-velocity diagram through the optical center along the kinematic major axis, however, and the sign of solid body rotation is evident.

4 Dark and Visible Matter in UGC 12695

Previous studies of the dark and visible matter of LSB galaxies have shown them to be extremely dark matter dominated with respect to “normal” HSB galax-

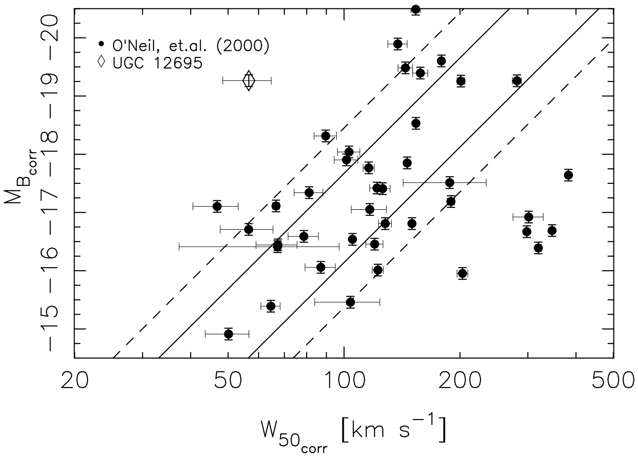

Figure 5: LSB galaxy Tully-Fisher relation. The lines are the 1σ and 2σ fits to the data of Zwaan, *et.al.*(1995), and the circles are recent observations of LSB galaxies in the Pegasus and Cancer groups from O'Neil, Bothun, & Schombert (1999). UGC 12695 (using i = 40°) is shown as a diamond.

ies (i.e. Van Zee, *et.al.*1997; De Blok & McGaugh 1997, 1998). Thus, although the lack of any turn-over in UGC 12695's rotation curve makes it clear that we have not come close to determining the full gravitational potential of the galaxy, it is still a worthwhile exercise to look at UGC 12695's total mass.

Classic Newtonian mechanics states that the dynamical mass of a rotating, gravitationally bound object is simply

$$M_{dyn} = \frac{v^2 R}{G \sin^2 i}$$

where G is the gravitational constant. Using the maximum known velocity of UGC 12695 (33/sin(40°) km s^{-1} at r=64"), this gives a total dynamical mass of 16 x $10^9 M_\odot$, while the determined H I flux gives a total H I mass of M_{HI} = 7.5 x $10^9 M_\odot$. Although at first glance these numbers hardly seem remarkable, they imply a considerable absence of dark matter for a LSB galaxy. Assuming a minimal disk scenario (M_*/L_B = 0), and letting all the gas in the galaxy be neutral hydrogen and helium ($M_{gas} = 1.47 \times M_{HI} = 11 \times 10^9 M_\odot$), gives a dark-to-total mass ratio of only M_{DM}/M_{dyn} = 0.30. Using somewhat more realistic numbers by letting M_*/L_B = 1, (a low-to-average LSB maximal disk value from Van Zee, *et.al.* 1997 & De Blok & McGaugh 1997) reduces the dark matter contribution to only 12% of the total dynamical mass of UGC 12695. (The luminosity value, $L_B = 2.86 \times 10^9 M_\odot$, is derived from the value given in O'Neil, *et.al.*, 1998 which used integrated aperatures. The error in L_B is less than 1%.) For comparison, the average M_{DM}/M_{dyn} values for LSB galaxies from De Blok & McGaugh is 0.6 for maximum disk scenarios, and for Van Zee, *et.al.* (1997) $\langle M_{DM}/M_{dyn} \rangle$ = 0.7. Additionally, if the stellar mass-to-light ratio of UGC 12695 is increased to 1.7, a reasonable value for both HSB and LSB galaxies, there is no need to invoke any dark matter to explain the maximum *observed* rotational velocity at the last measured point of UGC 12695's rotation curve. It should be noted that we were not able to observe any turn-over in UGC 12695's rotation curve. Thus, unlike the Van Zee, *et.al.* and De Blok & McGaugh samples we are not determining the dynamical mass from the flat portion of the rotation curve but instead from the still rising portion. As such, it is extremely likely that dark matter will play a large role in UGC 12695's outer regions.

It should also be noted that the *observed* velocity width of UGC 12695 causes it to fall well off the standard Tully-Fisher relation, lying approximately 2.5 magnitudes (3σ) above the LSB galaxy line defined by Zwaan, *et.al.* (1995) (Figure 5). This may be the consequence of the apparent lack of dark matter in the observed portion of UGC 12695. On the other hand, it is quite likely that there is significant dark matter outside the observed radius (else the rotation curve would show some turn over), and thus we are merely viewing a lower limit of the galaxy's rotational velocity. The uncertainty in UGC 12695's inclination (see the next section) also makes the current location of UGC 12695 on the Tully-Fisher relation suspect and if the inclination is less than 40° , UGC 12695 could move onto (or even to the right of) the Tully-Fisher relation of Zwaan, *et.al.*.

5 Star Formation in UGC 12695

It was demonstrated by Toomre (1964) that a thin, *collisionless* stellar disk in circular motion becomes unstable if the surface mass density exceeds a critical value of

$$\Sigma_c = \alpha \frac{\kappa\sigma}{3.36G}$$

where Σ_c is the critical density, σ is the velocity dispersion, α is a dimensionless constant near 1, and κ is the epicyclic frequency of the gas, also written as

$$\kappa = 1.41 \frac{V}{R} \left(1 + \frac{R}{V}\frac{dV}{dR}\right)^{1/2}.$$

Cowie (1981) showed that this criterion is also applicable to instabilities in a gaseous disk if embedded in a more massive stellar disk. Kennicutt (1989) determined an empirical value for α of about 2/3. Typical HSB galaxies exceed this critical surface density and form stars throughout most of their stellar disks.

As an LSB galaxy which appears to be in the midst of considerable but localized star formation, UGC 12695

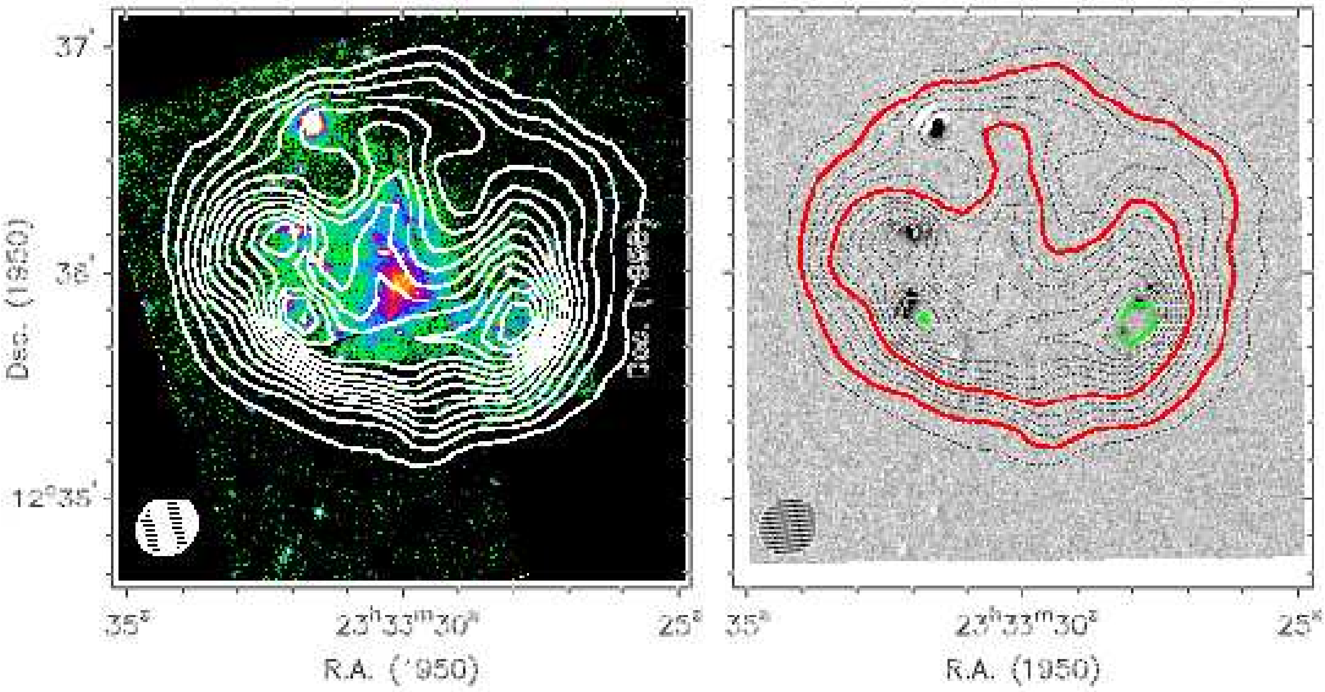

Figure 6: Left panel: HI contours of U12695 overlaid on the HST WFPC2 F814W image. Right panel: HI contours of U12695 overlaid on the Hα image. The red contours indicate the critical HI column density of 1.6×10^{20} and 6.0×10^{20} cm^{-2} above which star formation is expected based on Toomre's criterion (for i = 40° & 10° , respectively), while the green contours are the 10^{21} cm^{-2} level.

is an ideal case on which to test this star formation threshold theory. Before this can be done, though, κ and σ must be determined. From the rotation curve of UGC 12695 it is apparent that its near solid body rotation makes determining κ relatively easy. Approximating the rotation curve as pure solid body with an inclination corrected amplitude of 57 km sec^{-1} at a radius of 22 kpc yields κ=5.2 km sec^{-1} kpc^{-1} (using the fact that for a gas disk in pure solid body rotation, $\frac{dV}{dR} = \frac{V}{R}$ and $\kappa = \frac{2V}{R}$). Due to beam smearing the velocity dispersion is hard to measure from the data and a canonical dispersion of $\sim$8 km sec^{-1} is assumed as an average estimate (8 km sec^{-1} is also observed in several highly resolved face-on gas disks). This leads to a critical surface mass density of $\Sigma_c = 4.0 \times 10^{-3}$ kg m^{-2}. Taking a 32% helium mass fraction into account, this corresponds to a critical H I column density of 1.6×10^{20} atoms cm^{-2} (i.e. between the 1st and 2nd contours in Figure 6) above which star formation is to be expected. This implies that everywhere throughout the disk of UGC 12695 star formation should occur.

However, we only observe star formation in a limited number of localized regions near the very peaks of the H I column density distribution where it reaches levels of 1×10^{21} atoms cm^{-2}. This is illustrated in Figure 6 which shows in the left panel the HI column density map overlaid on a false-color WFPC2 F814W image and in the right panel the same H I contours overlaid on a greyscale MDM-1.3m Hα image. The lower red contour indicates the critical column density of 1.6×10^{20} atoms/cm^2. Obviously, the theoretically derived and empirically adjusted critical surface density is clearly not applicable to the low metallicity, irregular gas disk of UGC 12695.

One of the more curious aspects of the Kennicutt-Cowie-Toomre star formation criterion is that it successfully works at all, considering the number of physical processes which affect the value of Σ_c. For example, disks are not infinitely thin but have a certain thickness which could increase or decrease the column density thresholds and alter the radial instabilities. That is, if the volume gas density is significantly different than the surface gas density of UGC 12695, a volume-density dependent Schmidt law would be more appropriate than the Kennicutt/Cowie/Toomre star formation criterion used above (i.e. Ferguson, *et.al.* 1998). Additionally, there is energy dissipation, magnetic field lines, etc. which should also affect Σ_c (i.e. Hunter, Elmegreen, & Hunter 1998). Thus it is not surprising that UGC 12695, and in fact many LSB galaxies, do not adhere to the Toomre criterion (i.e. Van Zee, *et.al.* 1997; Van der Hulst, *et.al.* 1993).

What is interesting is that UGC 12695, like many LSB and dwarf galaxies, forms stars only where the

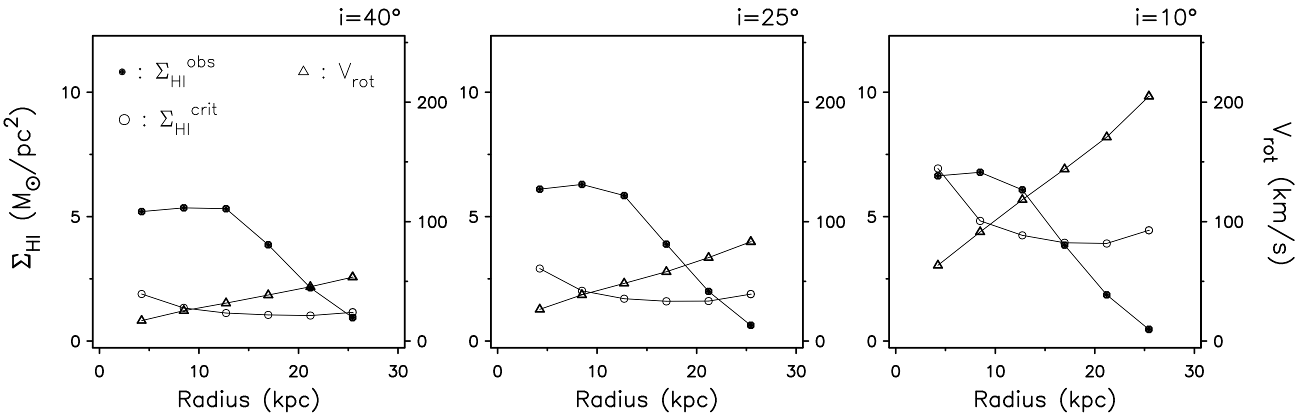

Figure 7: The azimuthally averaged observed gas density, Toomre star formation threshold, and rotation curves of UGC 12695 for an assumed galaxy inclination of 40° , 25° , and 10° (left to right).

local H I column density exceeds 10^{21} atoms cm^{-2}. In fact, Skillman (1986) pointed out that the actually observed *local* H I column density threshold for star formation, at a resolution of 500 pc, is about 1×10^{21} atoms cm^{-2} and roughly 5×10^{21} atoms cm^{-2} for star formation events of the order of 30 Doradus. This local H I column density threshold appears to be in better agreement with the observations of UGC 12695 (i.e. note the green contours in Figure 6), although the beam size makes a detailed analysis impossible. (The Hα data of McGaugh 1994 is not photometric, making determination of UGC 12695's H II luminosity difficult. It should be noted, though, that attempts to detect faint diffuse H-α regions have not been successful, making it unlikely that any widespread component of faint star-forming regions has been missed.)

Unlike our sample, a previous study by Van der Hulst, *et.al.* (1993) found their sample of low surface galaxies to be generally consistent with the Kennicutt-Toomre criterion for star formation. Perhaps the most important difference between this study of UGC 12695 and the Van der Hulst, *et.al.* results is that Van Der Hulst, *et.al.* used azimuthally averaged radial H I surface density profiles. Figure 7 shows the results of applying Van der Hulst, *et.al.*'s method to UGC 12695 for a variety of possible inclinations (see below). As can be seen, even by ignoring the extremely asymmetric nature of UGC 12695, only the most extreme case (*i*=10°) does UGC 12695 come close to falling below the critical density for star formation anywhere but in the outermost isophotes. This sort of study, though, disallows for any analysis of the local star forming potential of UGC 12695 while hiding the exceptionally asymmetric nature of galaxy.

At this point, it is important to consider the uncertainties involved in calculating Σ_C. Most notably, we should take another look at UGC 12695's assumed inclination. It is certainly possible that UGC 12695's shape truly is circular, thus validating the inclination value used in the previous calculations (40°). If, however, UGC 12695 has recently tidally interacted with UGC 12687, as discussed below, the perceived inclination may be overestimated in that UGC 12695 may have been distorted (and 'flattened') by the interaction (e.g. see Figure 2 of Mihos, *et.al.*, 1997). In this case the true inclination of UGC 12695 may be considerably less than we have assumed, thereby raising the value of Σ_C. As an example, if UGC 12695's true inclination is 10° , the critical density will increase to $\Sigma_C = 6\times10^{20}$ atoms cm^{-2}. In this case, although the critical density and the density at which star formation is observed still would not precisely coincide, they would lie considerably closer together (i.e. the higher red contour in Figure 6). If, in addition to the above correction to *i*, our estimate of κ is off by a factor of 60% (3σ) due to inclination uncertainties and the rotation curve shape, the critical density would readily be raised to 10^{21} atoms cm^{-2}, the observed local H I column density threshold for star formation of Skillman (1986). Of course, if the inclination correction is off in the other direction, and *i*=50° , Σ_C would be reduced even more, raising again the question of why UGC 12695 is LSB.

It is noteworthy to point out that the three local peaks in the neutral hydrogen of UGC 12695 lie near, but not on top, the primary star formation regions of the galaxy, as defined by the H-α image of McGaugh (1994). This is illustrated in Figure 8 which displays in the left panels the white VLA H I contours on the color WFPC2 F814W image, in the middle panels the yellow MDM-1.3m Hα contours on the WFPC2 image and in the right panels the combined H I and Hα contours on the WFPC2 image.

Figure 8 shows that there seems to be a clear offset between the highest peaks in the H I column density at 1.2 x 10^{21} cm^{-2} and the location of the primary Hα complexes. The largest star clusters seem to surround

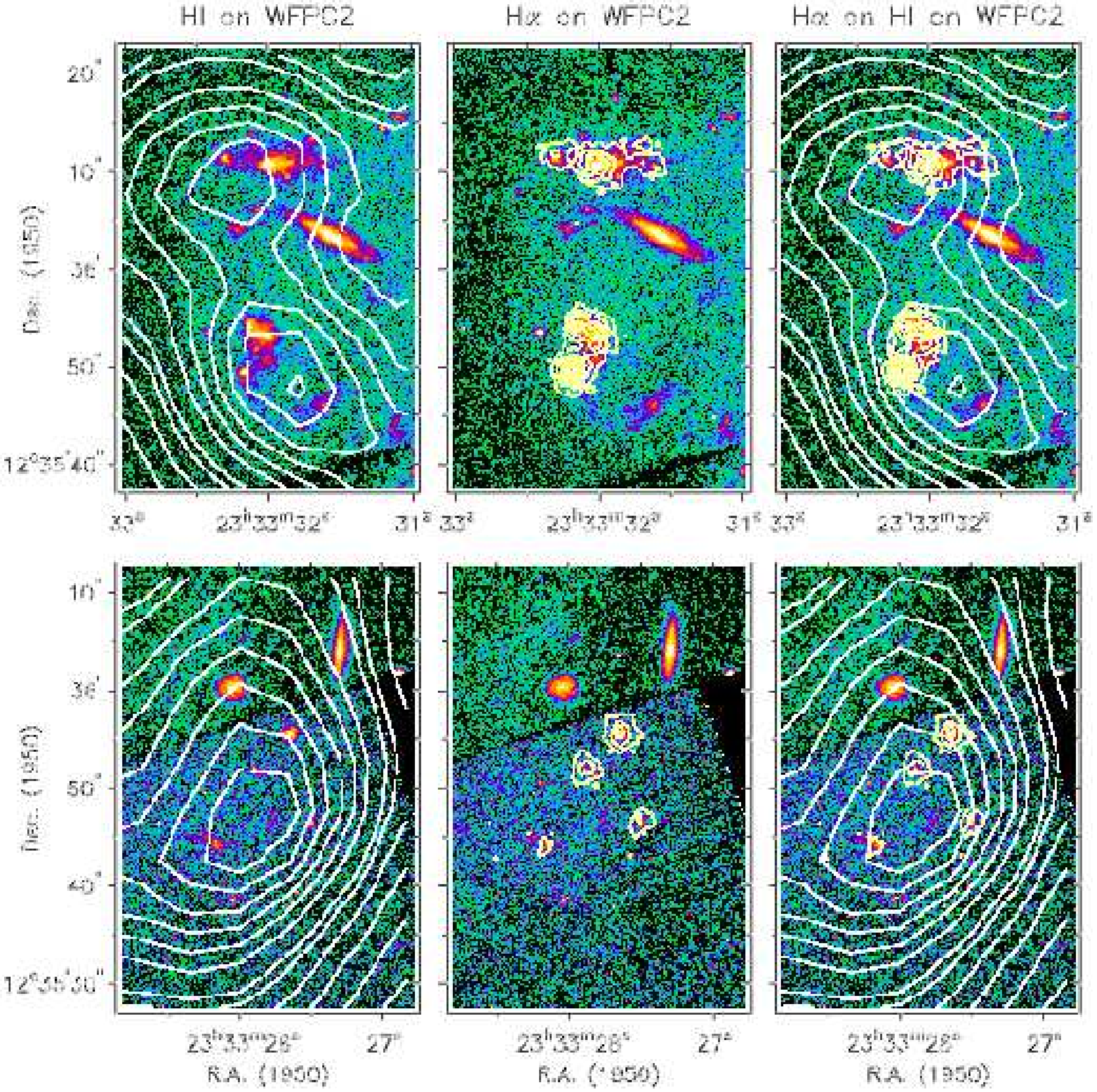

Figure 8: Zooming in on the main star formation regions in in UGC 12695. The upper row shows the star formation complexes in the eastern side of the galaxy. Those in the western side are shown in the bottom row. The white contours are from the VLA H I map while the yellow contours are from the MDM-1.3m Hα image.

the regions with the highest HI column densities. However, the relatively poor spatial resolution of the current H I observations is insufficient to draw any further conclusions on the relation between the H I peaks and the Hα regions.

The colors of those regions, as provided by the WFPC2 images, also put the star-formation peaks away from the H I peaks, with the left two H I peaks having F300W – F814W = –0.06 and –2.82, versus –3.27 and –3.14 for the corresponding H-α peaks (top and bottom, respectively). (These colors roughly correspond to U – I colors of 1.42, –1.34, –1.79. and –1.66, respectively (i.e. O'Neil, *et.al.*1998).) The third H I peak, at the bottom right of Figure 6, lies in the extremely noisy PC chip of the WFPC2 image, making the determination of colors in that region extremely difficult. Thus the neutral hydrogen is behaving as expected – as star formation occurs the surrounding gas is ionized, shifting the peak in the neutral hydrogen distribution to the edge of the star forming regions.

6 Are UGC 12695 and UGC 12687 Tidally Interacting?

The close proximity of UGC 12695 and UGC 12687 in redshift space, the lopsided morphology of UGC 12695 and its slightly skewed kinematics, immediately brings to mind the possibility of a tidal interaction (Figure 1). Additionally, the presence of 2333+1234 lying between the two galaxies suggests it may have been formed as a tidal remnant. (Of course, 2333+1234 may simply be a naturally occurring representative of the faint-end of the luminosity function.)

In 1997 Mihos, McGaugh, & De Blok argued that LSB and HSB galaxies of the same total mass are equally susceptible to local disk instabilities but that LSB galaxies are far less responsive to global instabilities than their HSB counterparts. This difference is mainly due to the stabilizing nature of the relatively more massive dark matter halo in which the LSB disk is embedded. To test their hypothesis, they modeled a strong prograde tidal encounter between an LSB and an HSB disk galaxy of similar mass. After the encounter the HSB galaxy exhibited two definitive spiral arms, a central inflow of gas and an oval central region. Presumably, the HSB system was in the midst of, or had recently undergone, a large burst of star formation in its core. Being more stable than its HSB counterpart, the LSB galaxy displayed a milder, yet significant response. Although the encounter strongly perturbed the LSB galaxy, it did not result in a central gas inflow. However, it did induce long-lived spiral arms, an overall lopsided distortion of the galaxy, and possibly localized compressions and instabilities in the disk.

The observed morphologies of UGC 12695 and UGC 12687 show a striking resemblance to the numerical simulations of Mihos *et.al.* at the time stamp T=36 (see their Figure 2). Their HSB system (UGC 12687 in our case) shows a strong bar from which two well defined spiral arms emerge. UGC 12687's observed morphology is in close agreement with their results while its central continuum emission and UV-excess indicate a considerable nuclear star formation activity, hinting at well developed bar kinematics efficient in fueling H I to the central region. In the case of the LSB galaxy, the numerical simulations display a sharp stellar edge on one side of the disk and a more diffuse gradient on the other side while a highly variable structure in the mass surface density hints at strong local instabilities. Observationally, UGC 12695's extremely blue colors, highly asymmetric gas and star distribution, and regions of intense local star formation also match the model predictions extremely well. In fact, without relying on some sort of external trigger the observed morphology and color of UGC 12695 is extremely difficult to explain.

In spite of the above assertions, a number of arguments against any major tidal encounter between these two galaxies must be considered. The first, and perhaps most obvious of these is the apparently settled kinematics of both UGC 12695 and UGC 12687. At first glance it would seem that if the two galaxies have interacted recently enough for the tidally-induced star formation to be at, or near, its peak the galaxies would still exhibit highly agitated kinematics. A study by Vázquez and Scalo (1989), though, has shown that starbursts do not typically occur during the gas compression stage but in fact occur well after the gas has re-established. In other words, the Vázquez and Scalo model suggests that disks can have tidally induced star formation well after the gas has kinematically re-settled.

A second argument which could be put forward against the idea of the two galaxies having recently undergone a tidal interaction is simply this – if UGC 12695 is experiencing a burst of localized star formation due to a recent tidal encounter, should it not be experiencing a corresponding rise in central surface brightness? A recent paper by O'Neil, Bothun, & Schombert (1998) tested this idea through modeling a wide variety of LSB galaxies experiencing localized starbursts. Their results were quite definitive – if a galaxy forms as a LSB galaxy, due to a high angular momentum giving rise to a low gas surface density etc., it will remain a LSB galaxy barring any major encounter catastrophe. Thus it is quite believable that UGC 12695 could be undergoing significant localized star formation activity and yet not be undergoing any significant change in its global surface brightness.

The final argument against UGC 12695 and UGC 12687 having undergone a significant tidal interaction in the recent past comes from examining the smoothed data cube. Not a trace of extended H I gas above a minimal detectable column density of 2×10^{19} atoms cm^{-2} (3σ) can be found besides the rotating gas disks of the three identified galaxies. This leads to the conclusion that no major tidal tails were ever formed in any past interaction between the two systems.

7 Conclusion

UGC 12695 is an intriguing low surface brightness galaxy of a very transparent nature, having an extremely blue color, a highly asymmetric appearance and very localized bursts of star formation near the peaks in the H I column density distribution.

Many of the properties of both UGC 12687 and UGC 12695 can be explained as being induced by such a tidal interaction, including the bar of UGC 12687 and its central radio continuum emission and UV excess as well as the lopsided appearance of UGC 12695 and the offset between its morphological and kinematic major axes. Furthermore, the localized bursts of star formation in UGC 12695 could very well be induced by such an interaction, giving rise to local instabilities in the LSB disk as demonstrated by Mihos *et.al.*(1997).

It is likely that UGC 12695 could have been living a fairly quiescent existence, its low surface gas density keeping its star formation rate quite low, and just now it is experiencing a period of localized but vigorous star formation triggered by a mild tidal interaction which might lead to a major morphological transition.

Within all this, though, it is easy to overlook one important fact. Although many of the properties of UGC 12695 and UGC 12687 can readily be explained through an ongoing tidal encounter, the two galaxies are still fundamentally distinct. UGC 12695 is not simply a fainter, or more 'stretched-out', or more quickly rotating version of UGC 12687. Were any of these the case the behavior of the two galaxies after the tidal encounter would be similar, and UGC 12695 would have experienced a central gas inflow with the majority of its star formation now occurring not in the outlying regions (as it is), but in the galaxy's core. Thus the fundamental question of why UGC 12695 is an LSB galaxy, and UGC 12687 is not remains unanswered.

8 Acknowledgments

The Very Large Array is a facility of the National Radio Astronomy Observatory, a facility of the National Science Foundation operated under cooperative agreement by Associated Universities, Inc. The Digitized Sky Surveys were produced at the Space Telescope Science Institute under U.S. Government grant NAG W-2166. The images of these surveys are based on photographic data obtained using the Oschin Schmidt Telescope on Palomar Mountain and the UK Schmidt Telescope. The plates were processed into the present compressed digital form with the permission of these institutions.

References

Condon, *et.al.*, 1998, AJ, 115, 1693

Cowie, L., 1981, ApJ, 245, 66

De Blok, W.J.G. & Van der Hulst, J.M., 1998, A&A, 336, 49

De Blok, W.J.G. & McGaugh, S., 1998, ApJ, 499, 41

De Blok, W.J.G. & McGaugh, S., 1997, MNRAS, 290, 533

Ferguson, H., & McGaugh, S., 1995, ApJ, 440, 470

Ferguson, A. *et.al.*, 1998, ApJ, 506, L19

Kazarian, M.A. & Kazarian, E.S., 1985, Afz, 22, 431

Kennicutt, R., 1989, ApJ, 344, 685

Hunter, D., Elmegreen, B. & Baker, A., 1998, ApJ, 493, 595

Matthews, L., & Gallagher, J., 1997, AJ, 114, 1899

McGaugh, S., 1994, ApJ, 426, 135

Mihos, C., McGaugh, S., & De Blok, W.J.G, 1997, ApJ, 477L, 79

O'Neil, K, Bothun, G., & Schombert, J., 1999, AJ, in press

O'Neil, K., Bothun, G., & Schombert, 1998, AJ, 116, 2776

O'Neil, K., *et.al.*, 1998, AJ, 116, 657

O'Neil, K., Bothun, G., & Cornell M., 1997b, AJ, 113, 1212

O'Neil, K., *et.al.*, 1997a, AJ, 113, 1212

Prugniel, P. & Heraudeau, P., 1998, A&AS, 128, 299

Schombert, J. *et.al.*, 1990, AJ, 100, 1533

Skillman, E.D., 1986, in "*Star Formation in Galaxies*", C.J. Lonsdale (ed), NASA Conference Publication 2466, 263

Theureau, G., *et.al.*, 1998, A&AS, 130, 333

Schneider, S., *et.al.*, 1990, ApJS, 72, 245

Toomre, A., 1964, ApJ, 139, 1217

De Vaucouleurs, G. *et.al.*, 1991, *The Third Reference Catalog of Bright Galaxies*, Springer-Verlag: New York

Van der Hulst, J.M., *et.al.*, 1993, AJ, 106, 548

Van Zee, L., *et.al.*, 1997, AJ, 113, 1618

Vázquez, E. & Scalo, J.M., 1989, ApJ, 343, 644

Zwaan, M., Van der Hulst, J., De Blok, W., & McGaugh, S.S., 1995, MNRAS, 273, L35